1

Growing bone tissue-engineered niches with graded osteogenicity:

an *in vitro* method for biomimetic construct assembly

Serena Danti[1,2,*], Lorenzo Pio Serino[3], Delfo D'Alessandro[1,2], Stefania Moscato[4], Sabrina Danti[1],

Luisa Trombi[2,4], Dinuccio Dinucci[5], Federica Chiellini[5], Andrea Pietrabissa[6], Michele Lisanti[3],

Stefano Berrettini[1], Mario Petrini[2,4]

[1] Dept. of Surgical, Medical, Molecular Pathology and Emergency Medicine, University of Pisa, via

Paradisa 2, 56126 Pisa, Italy

[2] Center for the Clinical Use of Stem Cells – Regional Network of Regenerative Medicine

"CUCCS-RRMR", University of Pisa, via Roma 55, 56126 Pisa, Italy

[3] Dept. of Translational Research and New Technologies in Medicine and Surgery, University of

Pisa, via Paradisa 2, 56124 Pisa, Italy

[4] Dept. of Clinical and Experimental Medicine, University of Pisa, via Roma 67, 56126 Pisa, Italy

[5] Dept. of Chemistry & Industrial Chemistry, via Risorgimento 35, 56126 Pisa, Italy

[6] Dept. of Surgical Sciences, IRCCS Policlinics San Matteo, University of Pavia, via Aselli 45,

27100 Pavia, Italy

* *Corresponding author's contacts:*

Serena Danti, Dept. of Neurosciences, via Roma 55, 56126 Pisa, Italy

Tel. +39 050 995033, Fax +39 050 997500, Email: s.danti@med.unipi.it

Contacts of co-authors:

delfod@interfree.it, lorenzo.serino@inwind.it: Tel. +39 050 995033, Fax +39 050 997500

s.moscato@med.unipi.it: Tel. +39 050 2218617, Fax +39 050 2218619

sabrina.danti@unipi.it: Tel. & Fax. +39 050 993556

l.trombi@med.unipi.it, mario.petrini@med.unipi.it: Tel. +39 050 993488, Fax +39 050 830162

federica@dcci.unipi.it, dinucci@ns.dcci.unipi.it: Tel:+39 050 2210305, Fax:+39 050 2210332

andrea.pietrabissa@unipv.it: Tel. + 39 0382 502536, Fax + 39 0382 502152

lisanti@med.unipi.it: Tel. +39 050 996527, Fax +39 050 996500

s.berrettini@med.unipi.it: Tel. & Fax. +39 050 997500

Running head: Biomimetic niches with graded osteogenicity

Abstract

The traditional bone tissue engineering approach exploits mesenchymal stem cells (MSCs) to be seeded once only on 3D scaffolds, hence differentiated for a certain period of time and resulting in a homogeneous osteoblast population at the endpoint. However, after achieving terminal osteo-differentiation, cell viability is usually markedly compromised. On the other hand, naturally occurring osteogenesis results from the coexistence of MSC progenies at distinct differentiative stages in the same microenvironment. This diversification also enables long-term viability of the mature tissue. We report an easy and tunable *in vitro* method to engineer simple osteogenic cell niches in a biomimetic fashion. The niches were grown via periodic re-seeding of undifferentiated MSCs on MSC/scaffold constructs, the latter undergoing osteogenic commitment. Time-fractioning of the seeded cell number during differentiation time of the constructs allowed graded osteogenic cell populations to be grown together on the same scaffolds (*i.e.,* not only terminally differentiated osteoblasts). In such cell-dynamic systems, the overall differentiative stage of the constructs could also be tuned by varying the cell density seeded at each inoculation. In this way, we generated two different biomimetic niche models able to host good reservoirs of pre-osteoblasts and other osteo-progenitors after 21 culture days. At that time, the niche type resulting in 40.8% of immature osteogenic progenies and only 59.2% of mature osteoblasts showed calcium content comparable to the constructs obtained with the traditional culture method (*i.e.,* 100.03 $\pm$ 29.30 *vs.* 78.51 $\pm$ 28.50 pg/cell, respectively; p = n.s.), the latter colonized only by fully differentiated osteoblasts showing exhausted viability. This assembly method for tissue-engineered constructs enabled a set of important parameters, such as viability, colonization and osteogenic yield of the MSCs to be balanced on 3D scaffolds, thus achieving biomimetic *in vitro* models with graded osteogenicity, which are more complex and reliable than those currently used by tissue engineers.

Keywords: mesenchymal stromal cell (MSC); niche; osteogenesis; biomimetics; cell seeding.

Introduction

Regenerative processes in living tissues draw on reservoirs of pluripotent cells, namely stem cells (SCs), which boast the unique skill of generating committed phenotypes able to progress along maturation, while maintaining their own stemness.[1] As a consequence, transit cellular progenies of the same lineage coexist at intermediate differentiative stages between the SC, upstream, and the terminally differentiated cell, downstream. In the bone tissue, fundamental regenerative phenomena, such as ossification, are ruled by osteoblastogenesis. Specifically, the osteogenic cascade is known to start following the activation of the mesenchymal stromal cells (MSCs), and to further progress across osteo-progenitor cells, pre-osteoblasts, osteoblasts, osteocytes and bone lining cells.[2] The complex mechanism of osteogenic differentiation of immature progenies is driven by chemical, biological and physical signals that control MSC activation, proliferation, migration, differentiation and survival. Most signals come from a peculiar microenvironment, also known as "niche", consisting of cell-secreted extra cellular matrix (ECM) molecules, where a broad-spectrum of cells lay, cross-talk and interact.[3]

In bone tissue engineering (TE), MSCs have been routinely employed for their superior proliferation, easier way of drawing and shorter time of isolation than those of osteoblasts.[4] For this application, MSCs have often been isolated from bone marrow (BM) (as they exhibit a high and well-established osteogenic potential) and have been expanded *in vitro* to obtain the desired cell number for seeding.[5] Typically, the *in vitro* TE approach adopts MSC/osteoprogenitor populations to be seeded on 3D scaffolds, cultured and differentiated using appropriate chemical supplements in the culture medium (CM).[6] These are sometimes combined with mechanical stimuli conveyed by bioreactors, aimed at enhancing the mineralized ECM formation.[7] The sooner have the cells seeded *in vitro* than they are exposed to a completely unknown environment which exhibits a complex architecture as well as differentiative stimuli other than those of their native conditions. Preliminary steps are to be considered, including MSC loss during seeding and adaptive cues.[8] At this point the survived cells, all at a similar early-stage of differentiation, are forced towards osteogenic

differentiation. Such a method may reveal to be effective in terms of final mineral matrix deposition, but it is still far from mimicking any physiological bone formation.[9] In addition, after the stress necessary to push undifferentiated cells towards maturation in a relatively short time-frame, most of them will either exhaust their replication capacity or die. Recently, developing biomimetic strategies have been envisioned as the most successful approach for creating functional complex tissues in the laboratory.[10] Researchers have started to investigate the key role exerted by the native ECM molecules and neighboring tissue population in bone TE, reporting that the microenvironment affects the MSC fate in different ways. In particular, depending on its composition, ECM retains the capability of either maintaining cell stemness[11] or conversely enhancing the osteogenic potential of MSCs.[12,13] Moreover, the initial cellularity of the samples is another important but often underestimated factor, further affecting the development of the MSC/scaffold constructs.[14,15] However, neither has the role performed by transient populations been deepened so far, nor have cell-dynamic biomimetic osteogenic niches been investigated in TE studies.

In this study, simple tissue-engineered osteogenic niches were assembled so as to progress towards the *in vitro* regeneration of biomimetic bone substitutes, which can be functional and viable at the time of implantation. The idea lying behind this study is the generation of a 3D niche hosting simultaneously a spectrum of cells at different osteogenic stages, which range from the undifferentiated MSCs to the terminally differentiated osteoblasts. We developed osteogenic niches consisting of human MSCs (hMSCs) cultured on 3D spongy scaffolds based on poly(L-lactic acid) (PLLA) and gelatin (G) (*i.e.,* PLLA/G). Such scaffolds were selected as they resulted to be highly suitable for both hMSC and osteoblast colonization on the basis of previous studies.[16-19] Coexistence of multistage osteogenic cells in the niches could be simply obtained by periodic seeding of undifferentiated hMSCs on hMSCs/scaffold constructs, the latter being cultured in osteogenic CM. In this way, owing to the time elapsed between each cell inoculation (*i.e.,* 5 days), we artificially created simple "cell-dynamic" systems in which osteogenic cell gradients evolving

with time have been generated. This system may represent a basic model designed to mimic bone tissue formation, in which MSCs periodically come from the BM to the surrounding bone surfaces and interact both with bone ECM molecules and different osteogenic cells living in the niche.[20] The system was investigated over three seeding groups with multiple cell inoculations (namely "multi-shot") and equal number of total seeded cells (*i.e.,* 500,000 cells/sample), but with different seeding densities per period: *(i)* single shot (= traditional method, *i.e.,* niche #3); *(ii)* multiple shots with decreasing cell densities (*i.e.,* niche #2); and *(iii)* multiple shots at equal cell densities (*i.e.,* niche #1) (Fig. 1). In the three cases, the initially seeded cells per scaffolds were 500,000, 250,000 and 125,000, respectively. Time-fractioning of the seeded hMSC number was hypothesized to result in niches with modulated extents of osteogenic cell fractions (*e.g.,* MSCs, progenitors, pre-osteoblasts, osteoblasts). Specific analyses were performed to evaluate the following parameters: *(i)* cell viability, *(ii)* scaffold colonization, *(iii)* bone-ECM molecule expression.

Materials and Methods

Expansion and culture of hMSCs

The BM-derived hMSCs used for this study were either supplied by Darwin Prockop Lab, Tulane Center for Gene Therapy (Tulane, LA, USA), or obtained from orthopedic patients of our hospital after informed consent.[16] HMSCs from both sources were preliminarily characterized in our laboratories and showed no appreciable differences in terms of osteogenic potential. According to the planned seeding schedule (Table 1), aliquots of hMSCs were defrosted from liquid nitrogen storage and plated in tissue culture polystyrene (TCPS) flasks at a cell density of 1,000 cells/cm^2 in order to reach the desired cell number in identical conditions (70% confluence, passage 2) at the scheduled times. HMSCs were expanded in regular CM containing: αMEM, 2 mM L-glutamine, 100 IU/ml penicillin, 100 μg/ml streptomycin (all from Invitrogen, Carlsbad, CA, USA) 16.5%

(v%) premium select fetal bovine serum (FBS) (Atlanta Biologics, Atlanta, GA, USA). All cell cultures were carried out in incubators under standard cell conditions, namely 37 ℃, 95% relative humidity, and 5% CO_2/95% air environment.

Scaffold fabrication

Biodegradable spongy scaffolds were fabricated based on poly(L-lactic acid) (PLLA; i.v. = 0.8, Lakeshore Biomaterials, Birmingham, AL, USA) and gelatin (G; Gelatin Type B, ~75 Bloom, from bovine skin, Sigma-Aldrich, St. Louis, MO, USA). PLLA/G scaffolds with a weight composition ratio of 91:9 were thus produced following an established procedure.[19]

Briefly, an aqueous phase containing 0.25% gelatin in ddH_2O was emulsified with a light organic phase containing 2% PLLA in chloroform (Sigma-Aldrich). The foam obtained was immediately quenched in liquid nitrogen and quickly freeze-dried until all the solvents were stripped out and a dry sponge was developed. Specimens were puncher-cut in discs (thickness = 1.5 mm; diameter = 6 mm; weight ≈ 16 mg), sterilized by ethylene oxide gas, pre-wetted using absolute ethanol (Carlo Erba Reagents, Milan, Italy) under centrifugation, equilibrated in phosphate buffered saline (PBS; Sigma-Aldrich) and air-dried under laminar flow for 1 h.

Culture of hMSC/scaffold constructs

Sterilized scaffolds were press-fit into sterile silicon-molded holders, customized for these scaffolds, and placed in low-attachment 6-well TCPS culture plates (Cellstar, Greiner Bio-one, Frickenhausen, Germany). Before seeding, hMSCs were counted by a Coulter Counter (Coulters Multisizert 3, Beckman Coulter, Miami, FL, USA), taking an average over 3 measurements. Trypan blue dye (Sigma-Aldrich) at 0.2% (final sample concentration) was then used to evaluate the cell viability percentage. Cells were appropriately diluted in order to have cellular suspensions leading to the desired seeding density of viable cells *per* scaffold in a 200 µl volume.

The experimental design consisted of 3 seeding groups, each of which was composed of 6 scaffolds ($n = 6$). The groups were seeded with different seeding densities per period, as shown in Table 1. At subsequent seeding times, the osteogenic CM (*i.e.,* regular CM at 10% FBS, supplemented with 10^{-7} M dexamethasone, 10^{-2} M β-glycerophosphate, 50 μg/ml L-ascorbic acid, 0.1 ng/ml fungizone, all from Sigma-Aldrich) was removed from the top of the cassettes, hMSCs were seeded and let to adhere for 1 h, and then regular CM was added for 24 h. For all groups the culture was carried out for 21 days, *i.e.,* 16 days in osteogenic CM. After the last seeding time-point (t_3), all constructs were released from the cassettes and freely placed inside TCPS 6-well plates until the endpoint (t_f). The study design appears in Figure 1.

Cell colonization and viability in the niches

Neutral red (NR) assay

Cell viability and cell colonization of the scaffold surfaces were qualitatively investigated using a non-disruptive assay based on neutral red (NR; Sigma-Aldrich).[21] The day following both the first and the last cell inoculation [*i.e.,* (t_0 + 1 day) and (t_3 + 1 day), respectively], one specimen for each group was incubated with 50 μg/ml of NR in expansion CM for 1 h. Samples were rinsed in sterile PBS and their surfaces were observed under stereomicroscopy. After observation, PBS was replaced with CM and the culture was continued up to the endpoint.

Live/Dead® assay

The Live/Dead® viability/cytotoxicity kit (Molecular Probes, Eugene, OR, USA) was used to assess the 3D spatial distribution of cells at the endpoint (t_f). The constructs were rinsed with PBS and incubated at 37 °C for 30 min in the dark with the fluorescent medium, consisting of 1.2 μM calcein AM and 2 μM EthD-1 in PBS. CLSM (Zeiss LSM 510 Axiovert, Carl Zeiss, Germany) was employed to image the constructs under an Argon laser excited at 488 nm with emitted light collected at 515 nm for calcein AM and 635 nm for EthD-1. Stacks of confocal optical sections

were acquired at 4 μm intervals. Cells in 3D cell/scaffold constructs were rendered with a depth code associated to their depth-location.

Image analysis

ImageJ software (version 1.44, NIH, Bethesda, USA) was used to process the images of the CLSM optical sections.[22] The histogram of each color intensity was computed in each sample, for each slice, for each channel (green for live cells, red for dead cells and white for empty volumes). The logarithmic value (*ln*) of the pixel counts was calculated at maximum intensity. The R package (R Development Core Team, 2005) was employed to perform a polynomial (2nd order) regression analysis of the series.[23]

Scanning Electron Microscopy (SEM) analysis

Samples ($n = 2$) at 2 time points, *i.e.,* ($t_0 + 1$ day) and (t_f), were processed for SEM analysis as described earlier.[16] The dried samples were cross-sectioned, sputter-coated with gold (Sputter coater Emitech K550, Quorum Technologies Ltd, West Sussex, UK) and examined on a Quanta scanning electron microscope (FEI, Hillsboro, OR, USA).

Scaffold cellularity and seeding efficiency

HMSC number (or cellularity) was determined measuring the double strand (ds) DNA content using the PicoGreen kit (Molecular Probes, Eugene, OR, USA) according to published methods.[24-25] Cellularity was calculated dividing the measured value of ds-DNA by the nuclear DNA content of a human diploid cell (7.18 pg/cell).[26] One hour after each seeding event, a set of samples was used to evaluate the efficiency of the scaffold-cassette seeding system by collecting the CM and quantifying the unattached cell number. Total seeding efficiency was then calculated as the percentage ratio of the seeded cell number to the number of cells suspended.

For quantitative assays, 4 constructs for each group ($n = 4$) were collected at the endpoint (t_f) and lysed via freeze-thawing-sonication cycles, as previously reported.[24]

Osteogenic differentiation of the niches: quantitative analyses

Alkaline Phosphatase (ALP) Activity

Intracellular ALP activity was quantified in cascade on construct lysates assayed for cellularity ($n = 4$) by means of a colorimetric endpoint assay based on *p*-nitrophenol, using the reagents provided by Sigma-Aldrich.[27] The absorbance increase at 405 nm allowed the enzyme activity to be quantified in the samples, as previously reported.[25] ALP activity was normalized by cellularity.

Calcium Content

Calcium content in construct lysates ($n = 4$) was quantified using a colorimetric endpoint assay based on Arsenazo III (Diagnostic Chemicals Ltd., Oxford, CT, USA), according to a published method.[24] This assay measures at 650 nm the amount of blue-purple-colored Ca-Arsenazo^{++} complex, formed when Arsenazo III binds to free Ca in acid solution. Ca content was normalized by cellularity.

Osteogenic differentiation of the niches: qualitative and semiquantitative analyses

Cell morphology and calcium imaging via CLSM

A set of samples was treated with 10 μg/ml tetracycline HCl (Sigma-Aldrich) to assess mineral matrix formation under CLSM.[28,29] At the endpoint, samples were fixed in 4% buffered formalin and incubated with a 0.01 M solution of 4'-6'-diamidino-2-phenylindole (DAPI; Invitrogen) and phalloidin-Alexa633 (Invitrogen) for 45 min at RT. A laser diode (405 nm emission), Argon ion laser (488 nm emission) and Helium-Neon laser (633 nm emission) were used for excitation of the 3 fluorophores.

Histological analysis

Samples were processed for histology, as previously reported.[16] The sections, 8 μm thick, were stained with a specific kit for Alcian Blue (Bio-Optica, Milano, Italy), according to the manufacturer's recommendations.

Bone proteins were immunodetected using a streptavidin revelation kit (Vectastain Elite ABC Kit Standard, Vektor Lab, Burlingame, CA, USA), as described earlier.[16] For osteopontin (OPN), osteocalcin (OCN) and collagen I (Coll I), the sections were permeabilized with 0.2% Triton solution (Sigma-Aldrich), while an unmasked buffer (Diapath S.p.A, Bologna, Italy) was used for Runx2. The following primary antibodies were used: mouse monoclonal anti-OPN (Santa Cruz Biotechnology, Santa Cruz, CA, USA), rabbit polyclonal anti-OCN (Santa Cruz Biotechnology), rabbit polyclonal anti-Coll I (AbCam, Cambridge, MA, USA) mouse monoclonal anti-Runx 2 (Abnova, Taipei, Taiwan). Micrographs at $40\times$ optical magnification (total magnification $400\times$) were captured for each niche-type to evaluate cell morphology, number of antigen-positive cells and to score antigen intensity. Averages of about 600 cells were counted and analyzed for each group. Antigen positivity was scored by 3 independent observers according to the following criteria: 0 = negative; 1 = weak positivity; 2 = good positivity; 3 = strong positivity; 4 = very strong positivity.

Statistical analysis

For image analysis, a unique regressive model was built for each sample, able to fit both the green and the red series, using a centering method to minimize the autocorrelation impact. Significance of each model and normality of the residuals were checked out by the Jarque-Bera and Shapiro-Wilk tests. The confident intervals (95% of variance) of the models could thus be calculated to compare green and red series along the depth levels.

Elsewhere, statistical analysis was conducted using Welch's test to adequately manage samples having unequal variances. The results were corrected for multiple comparisons using the

Bonferroni-Holm method. Data underwent both descriptive [mean ± standard deviation (SD)] and inferential statistics (p values).

Results

Cellular viability, colonization and morphology

Cell viability on the top surfaces of the niches

The NR assay, performed on the same samples at two different time-points (2nd and 16th culture day) highlighted the presence of viable cells on the top surfaces of the constructs (Fig. 2). At those times, the niches had just received 1 and 4 seeding shots, respectively. Stereomicroscopy analysis revealed interesting differences between the samples. At the first time of observation ($t_0 + 1$ day), the extent of cell viability on the top surfaces of the niches reflected the densities of cell seeding, being the lowest in niche #1 and the highest in niche #3 (Fig. 2 A1-C1). Instead, at the last time of observation ($t_3 + 1$ day), niches #1 and #2 displayed a higher top colonization of viable cells than niche #3 (Fig. 2 A2-C2). Specifically, in niche #1 the viable cells were found to be very concentrated in the center of the scaffold 1 day after the first seeding (Fig. 2 A1) and homogeneously diffused all over the top surface after the last seeding (Fig. 2 A2). The same trend was observed in niche #2, in which the cells, initially seeded at a double concentration (Fig. 2 B1), could spread out over the whole surface following the subsequent seeding shots (Fig. 2 B2). Differently, in niche #3, where no additional seeding was performed with time, cell viability on the top surface was significantly reduced on day 16 (Fig. 2 C1-C2).

Cell viability inside the niches

The Live/Dead® assay allowed images of both live and dead cells to be obtained via CLSM up to about 200 μm depth, which were rendered using the "depth code" mode (Fig. 3 A-B). Live cell colonization in the niches was reported in Figures 3 A1-3, dead cell localization in Figures 3 B1-3.

13

From this qualitative evaluation, it was possible to visualize a massive presence of live cells in the investigated thickness of all samples. Moreover, the presence of dead cells was detected in the same volumes although at a lesser extent than that of live ones. In such samples, a qualitative comparison was very difficult and presumably would have been misleading; therefore, we devised an image analysis method to comment these data.

Image analysis performed on the CLSM sections revealed that the color levels displayed a statistically significant difference within the same niche (ANOVA Bonferroni-corrected; $p<0.0001$), while this difference was not statistically significant when the same color levels were compared between the three niches ($p=0.2$, n.s.). This means that the obtained data can only be used for intra-niche analysis (Fig. 3 C1-3). In the centered series, normality of the residuals was checked by the Jarque-Bera test, discovering that the null hypothesis of normal distribution of the data could not be rejected (JB test $p>0.09$). However, a statistically significant effect of the factor interaction (color$\times$sample, $p=0.0001$) was found. The white channel resulted as a linear constant in each sample, allowing intra-sample comparison between live and dead cells. The resulting regressive models for the live and dead cells are shown in Table 2. The models and their confident intervals were calculated and compared within each sample, as reported in Figure 3C. The boundaries of green and red series never overlapped only in niche #2, making the differences between viable and dead cells significant for only this niche (Fig. 3 C2).

Cell colonization and morphology inside the niches

The results of SEM analysis are reported in Figure 4. Micrographs of constructs showed the cellular colonization in the three niches (magnification 200$\times$) (Fig. 4 A-C), at ($t_0 + 1$ day) (Fig. 4 A1-C1) and at (t_f) (Fig. 4 A2-C2). Cell morphology and ECM production by osteo-differentiated hMSCs at the endpoint (t_f) were also shown (magnification 1,000$\times$) (Fig. 4 A3-C3). At (t_0+1 day), the hMSCs were found to be lying at the top of the scaffolds and displaying a flat and smooth morphology, which was similar in all the niche-groups (Fig. 4 A1-C1). Owing to the different number of seeded

cells, incomplete colonization was observed in niches #1 and #2, while niche #3 was almost fully covered by a cell layer (Fig. 4 A1-C1).

Cells could be found in the cross-sections at the endpoint (t_f) of all samples (Fig. 4 A2-C2). However, colonization in niche #1 was still incomplete (Fig. 4 A2). In this niche, the cells mostly appeared in spindle-like rather than round shape, and basic ECM production could be observed (Fig. 4 A3). By contrast, niche #2 showed a high cellular density (Fig. 4 B2), and cells with elongated or round-shaped morphology could be observed (Fig. 4 B2-B3). Evidence of protein synthesis could also be seen (Fig. 4 B3). Colonization in niche #3 appeared to be concentrated in cell-dense volumes mainly at the center of the scaffold (Fig. 4 C2). Here, all cells displayed a round morphology and production of intercellular ECM was abundantly revealed (Fig. 4 C3).

Niche cellularity

Using the scaffold-customized cassettes, the estimated seeding efficiencies were 91.08%, 93.27%, 90.49% in niche #1, #2, #3, respectively (Table 1). Cellularity quantified at the endpoint is shown in Figure 5A. Calculated cell numbers were: 266,415 $\pm$ 43,830, 228,106 $\pm$ 31,002 and 300,529 $\pm$ 81,265 cells/sample, for niche #1, #2 and #3, respectively (Fig. 5 A). However, no statistically significant difference could be detected among the three niche-groups ($p>0.05$).

Osteogenic differentiation of the niches

Osteogenic biomolecules: Quantitative analyses

The outcomes of the intracellular ALP activity assay are given in Figure 5B. The enzyme was present and active in all the niches, with the following values: 0.125 $\pm$ 0.027, 0.149 $\pm$ 0.012 and 0.117 $\pm$ 0.030 pmol/(h·cell), in niche #1, #2 and #3, respectively, with no statistical difference among the niches ($p>0.05$) (Fig. 5 B).

Results of calcium content are shown in Figure 5C. Ca^{++} quantity in niche #1 was 25.53 $\pm$ 22.90 pg/cell, while it was 100.06 $\pm$ 29.30 and 78.51 $\pm$ 28.50 pg/cell in niches #2 and #3, respectively.

Statistically significant differences were detected between niches #1 and #2, and between niches #1 and #3 (in both cases, $p<0.01$). No statistically significant difference was found between niches #2 and #3 ($p>0.05$) (Fig. 5 B).

Osteogenic biomolecules: Histomorphological analyses

Presence and specific localization of the ECM molecules and of the main markers involved in the osteogenic differentiation of hMSCs were investigated using histochemical, immunohistochemical and CLSM analyses (Fig. 6). Semiquantification of the protein markers is summarized in Figure 7, in which the detected proteins are grouped in relation to cell number, cell morphology (spindle-*versus* round-shaped cells) and, in some cases, to their localization (nuclear *versus* cytoplasm, or intra- *versus* extra-cellular). In particular, Figure 7A summarizes that niches #1 and #2 (*i.e.,* periodically seeded niches) display cells with two well-distinguishable morphologies (with 79.9% and 40.8% spindle-like cells, respectively), while niche #3 only contains round-shaped cells. Alcian Blue staining at pH 2.5 showed the presence of generic GAGs (in cyan), which were homogeneously detected both at intra- and extra-cellular levels in niche #3 (Fig. 6 A3) and to a lesser extent in niche #2 (Fig. 6 A2), while GAGs in niche #1 showed a low expression, which could be more rarely observed at an extracellular level (Fig. 6 A1).

Protein markers were investigated via immunohistochemistry. The Runx2 expression appeared in both the nuclei and the cytoplasm, showing its highest positivity at the nuclear level, with the exception of the round-shaped subpopulation in niche #2 (Fig. 7 B). Specific differences related to cell morphology could be highlighted among the niche types. In niche #1, Runx2 protein was expressed only in spindle-shaped cells (Fig. 6 A2 and 7 B) with nuclear intensity of 2.56 ± 1.06 and cytoplasmatic intensity of 0.85 ± 0.35. Differently, in niche #2, Runx2 was immunodetected in both cell morphotypes, and expressed in an opposite fashion. In the round-shaped cells, the Runx2 appeared mostly in the cytoplasm, while in elongated cells mostly in the nucleus (Fig. 6 B2 and 7 B). Specifically, the intensity of cytoplasmatic positivity was 0.69 ± 0.46 in spindle-shaped and

3.08 ± 0.05 in round-shaped cells), while intensity of nuclear positivity was 2.08 ± 1.39 in spindle-shaped and 0.50 ± 1.33 in round-shaped cells; both comparisons showed statistical significance ($p<0.0001$). In the round-shaped cells of niche #2, Runx2 showed a highly heterogenic expression at the nuclear level, being either zero in 87% or 4 (top score) in 13% of nuclei. In niche #3, all cells showed round morphology and high Runx2 immunopositivity, with 4.10 ± 0.04 at nuclear and 3.02 ± 0.06 at cytoplasm level (Fig. 6 C2 and 7 B). Lastly, inter-niche comparisons between elongated cells revealed that the highest positivity intensity was in in niche #1, both at nuclear ($p<0.005$) and cytoplasm level ($p<0.004$). Conversely, inter-niche comparisons among round cells, showed that the highest Runx2 nuclear intensity occurred in niche #3 ($p<0.0001$), while cytoplasmatic intensity was not statistically different (p=n.s.) (Fig. 7 B). Summarizing, a cell-heterogenic expression of the Runx2 protein was slightly observable in niche #1 (where the round cells appeared to be completely immunonegative) and mostly in niche #2 (where distinct cell populations displayed a different immunopositivity localization).

OPN was immunodetected in all niches (Fig. 6 A3-C3 and 7 C). Round-shaped cells were allover strongly OPN-immunopositive (positivity intensity: 3.03 ± 0.05, 3.11 ± 0.04 and 3.09 ± 0.05, in niche #1, #2 and #3, respectively; p=n.s. in all the comparisons), with both cytoplasmatic and extracellular localizations, while spindle-shaped cells showed characteristic perinuclear localization (2.18 ± 0.76 and 0.98 ± 0.13, in niche #1 and #2, respectively) and reduced immunopositivity in niche #2 ($p<0.0001$) (Fig. 7 C). In this case, a graded positivity of the OPN protein could be observed in elongated cells. The results of intra-niche comparisons (spindle *versus* round cells), showed that OPN was all over the most intense in the round cells ($p<0.0001$).

Coll I was immunodetected both at the intra- and extra-cellular levels in all the niches, but with important differences ranging from partial immunonegativity of niches #1 to abundant extracellular secretion of niches #3 (Fig. 6 A4-C4). In niche #1, Coll I was synthesized with low and heterogeneous positivity (Fig. 6 A4). The elongated cells showed this marker sometimes at the extra- and more often at the intra-cellular level, with intensity of 1.25 ± 0.56 and 0.58 ± 0.18,

respectively (Fig. 7 D). In round cells, the positivity intensity was 0.25 ± 0.25 at the intra- and 0.75 ± 0.76 at the extra-cellular level (Fig. 7 D). In this niche, the intracellular Coll I intensity was higher in elongated cells than in round cells ($p<0.0001$), while no statistically significant difference was found at the extracellular level (p=n.s.) (Fig. 7 D). In niche #2, elongated cells expressed Coll I antigen at the intracellular level (1.02 ± 0.05), without statistically significant difference against niche #1 (p=n.s.). However, the highest extracellular expression (2.00 ± 0.04) of this protein in niche #2 was revealed within the intercellular areas of round-shaped cells (Fig. 7 D), where well-defined interconnected filaments of Coll I could be observed (Fig. 6 B4). In niche #2, round cells displayed Coll I intensity significantly higher than in niche #1 at both the intracellular ($p<0.0001$) and the extracellular levels ($p<0.0001$) (Fig. 7D). Finally, niche #3 displayed the strongest extracellular immunopositivity for Coll I (4.09 ± 0.05; $p<0.0001$) among the three niches (Fig. 7 D). At intracellular level no statistically significant difference was detected against niche #2. In this niche, a dense network of collagen fibrils embracing round cells was highlighted (Fig. 6 C4).

OCN was immunodetected in all niches (Fig. 7 E), but with different localization and immunopositivity (Fig. 7 E). In niche #1, OCN was weakly expressed (1.06 ± 0.06) only in elongated cells at intracellular level (Fig. 6 A5). In addition to a similar OCN expression by spindle-like cells, niche #2 displayed a round-cell population with strong OCN-immunopositivity (3.04 ± 0.05), localized mainly at the cytoplasm and more rarely at the extracellular level (Fig. 6 B5). The presence of these two populations with different immunopositivity and localization of OCN rendered the niche #2 yield less positive on the whole than that of niche #3, in which only round cells were present. These cells showed OPN positivity comparable to that of niche #2 (3.00 ± 0.05), in addition to a wider extracellular localization of this antigen than that detected in niche #2 (Fig. 6 C5). No statistical differences were found in inter-niche comparisons of the same morphotypes (p = n.s.). However, owing to the coexistence of two distinct cell populations (elongated and round cells), each one retaining a specific expression of this antigen, niche #2 was the only one in which the expression of this biomolecule was found to be diversified ($p<0.0001$).

Finally, the calcium matrix formation was highlighted via CLSM (Fig. 6 A6-C6). Calcium deposits were enhanced in all the niches in proximity of round cells, although they were encountered only sporadically in niche #1, suggesting a reduced amount of mineralization. In particular, elongated cells with large nuclei and well-defined f-actin filaments mixed with smaller round cells could be observed in niches #1 and #2 (Fig. 6 A6-B6). Finally, the cells in niche #3 were round and small, showing DNA condensation and poor f-actin development (Fig. 6 C6).

Discussion

The conventional TE approach exploits MSCs to be inoculated on 3D scaffolds with static (*e.g.,* droplet) or dynamic methods and therein differentiated.[30] However, after achieving *in vitro* terminal osteo-differentiation, including a large production of calcium matrix in the short timeframe of a few weeks, osteoblast viability and synthetic activity are usually exhausted. On the other hand, naturally occurring osteogenesis results from the coexistence of MSC-derived progenies at distinct differentiative stages which form a complex and intercommunicating microenvironment with their ECM. This diversification of osteogenic cells also enables long-term viability and self-renewal of the mature tissue *in vivo*.[31] Bone formation thus relies on the concept of "niche", which is considered as a dynamic SC-matrix microenvironment providing both self-renewal and specific differentiating stimuli.[3,20] The use of biomimetic approaches has been proposed in recent years as a key factor for engineering functional tissues *ex vivo*.[9,10] Indeed, the novel TE strategies should *"try to fabricate scaffolds or create microenvironments that mimic these metastable tissues and promote complex cell–cell and cell–matrix interactions, rather than precisely engineer the final tissue form"*.[10] It is a fact that in its initial decades TE has widely employed *"minimalistic approaches based on homogenous populations of cells provided with suitable environmental conditions to give rise to specific practical outcomes (e.g., mineralized scaffolds..)"*.[9] However, it is of general

understanding that the regeneration of functional tissues, for their intrinsic complexity, will necessarily have to be based on more advanced *in vitro* models than those achieved so far.

Our study is aimed at going a step further in this direction, creating simple osteogenic cell niches hosting a gradation of mesenchymal-origin bone cells by means of an easy and tunable *in vitro* method able to engineer simple osteogenic cell niches in a biomimetic fashion. In this report, basic *in vitro* models of osteogenic 3D niches were obtained by periodic seeding of undifferentiated hMSCs on osteoinduced hMSC/scaffold constructs. Such an experimentally simple method allows diverse osteogenic cells to be developed on the same scaffold. Moreover, the arrival of new immature cells at an osteogenic niche mimics in a simple way the cell turnover in non-hematopoietic BM compartments, where undifferentiated cells constitutively present in the BM, come into contact with adherent osteogenic cells, which are attached to the neighboring bone surfaces, and differentiate.[20] Although still largely incomplete (*e.g.,* the hematopoietic and the endothelial cells are missing), our cell-dynamic system is actually far too complex to be evaluated during its development, as discontinuity points due to the seeding events are present which would affect measurements over time. Therefore, in this paper we only focus on the comparison of 3 niche types at a selected endpoint (*i.e.,* 21 culture days, 16 osteo-induction days), all of them having received the same number of cells (*i.e.,* 500.000 cells/sample).

The importance of finding appropriate methods for MSC seeding has also been pointed out by several authors looking for optimization of their tissue constructs;[14,30,32] however, the seeded cell number should always be considered a decisive parameter to be taken into account, as it affects the cell loss at seeding (*i.e.,* the real cell density achieved *per* scaffold area) together with the scaffold specific architecture and material and surface properties.[33] Cell-cell signals have indeed proved to be extremely important in cell proliferation, migration and ECM molecule deposition and either too high or too low densities may be equally detrimental to achieve the desired neo-tissue formation.[9]

In our model, long-term viability of the periodically seeded niches (niches #1 and #2) seemed to be confirmed by our observations: on the top surfaces, the viable cells detected by the NR assay

increased with respect to the use of the traditional method. An attempt to determine the viability of the constructs in the third dimension was performed using the Live/Dead® assay under CLSM. The presence of both live and dead cells in the three niches could be highlighted via CLSM up to its detection threshold (about 200 μm). However, since a qualitative inter-niche comparison of these phenomena resulted very difficult, we performed image analysis of the samples for each slice (*i.e.,* depth level) and for each color channel (*i.e.,* green and red, for live and dead cells, respectively) by computing the histogram of the colored pixels at the maximum intensity. This method made it possible to extract additional information from those images. First of all, only intra-niche differences between live and dead cells could be identified. Moreover, a statistically significant difference between live and dead cell numbers was detected only for niche #2. Finally, the cellularity data obtained by ds-DNA quantification, which cannot discriminate between live and dead cells, were not statistically different in the three niches, corroborating the consistency of our seeding method. Colonization of the three niches in cross-sections was also confirmed by SEM analysis conducted at the endpoint. All in all, this set of analyses highlighted that multiple-seeding methods allowed increased cell viability and homogeneous colonization of the seeding surface with respect to the traditional method. On the other hand, inner colonization in these scaffolds seemed to be pulsed by higher initial cell densities (250,000 and 500,000 cells/shot). Among the 3 niche-groups, niche #2 accounted for the highest surface viability, most regular inner colonization and statistically significant difference between live and dead cells over the third dimension.

From the osteo-differentiation standpoint, the ALP activity was similarly expressed in the three niches, while calcium content in both niches #2 and #3 was almost 4 times higher than in niche #1, with statistical significance, clearly indicating bone maturation of these constructs.[34] It is interesting to note that multi-seeded niches resulted in high seeding efficiency (>90%) and fairly homogeneous quantitative results (*i.e.,* standard deviations not higher than in niche #3). Differently, niche #3 was the most heterogeneous in terms of Ca^{++} content. Therefore, a multiple-shot (in this case, $s=4$ shots) method can also offer advantages in seeding efficiency, decreasing the risks associated with a single

seeding event (s=1). As a matter of fact, the subsequent seeding events may favor the achievement of more homogeneous cell distribution and differentiation in all three dimensions in a reproducible manner. Improvement of seeding efficiency and spatial distribution of seeded cells has also been reported to occur in bioreactors used for cell seeding under oscillating flow (s>>1).[33,35]

Histology and SEM highlighted subpopulations with two different morphologies (spindle-like and round) in niches #1 and #2, while only round cells were observed in niche #3. Niche #1 mainly showed elongated cells (about 80%), expressing high positivity for Runx2 and OPN, and low levels of Coll I and OCN. Calcium was present but in reduced amount with respect to the other niches, thus indicating that it was the most immature niche type.[36] In niche #2, the two subpopulations were more balanced (elongated- *vs.* round-cell ratio about 2:3) and osteogenic antigens were well diversified according to cell morphology. In particular, an enhanced expression of OCN, Coll I fibers and nuclear-level Runx2 were found in round cells, while high cytoplasmatic expression of Runx2 was shown by the elongated cells. Finally, niche #3 showed round cells (100%) with the highest positivity among all the investigated osteogenic proteins.[37] However, chromatin condensation, was revealed, which is a sign of cell sufferance and apoptosis.[38] Finally, it should be observed that calcium content in niches #2 and #3 was not statistically different. However, only niche #2 still had a reservoir of non-terminally differentiated cells (*i.e.,* spindle-like cells) able to maintain self-renewal and to carry on further ECM maturation or remodeling. Considering that the average residence time of cells (*i.e.,* the average time hMSCs were exposed to osteogenic CM) in niche #2 was shorter than in niche #3 (weighted mean of culture times: 16.7 days *versus* 21 days), our results indicate that the niche microenvironment has played a role in the osteogenic commitment of hMSCs.

Conclusions

The periodic addition of undifferentiated cells inside a differentiative environment is a simple method that permits osteogenic cell gradients to be generated within the resulting population.

Moreover, via periodic seeding, a biomimetic cell-dynamic niche model can be created, where hMSCs periodically come and interact with both bone ECM molecules and other previously generated osteogenic cells. Variation of cell densities of the seeding shots (*i.e.,* time-fractioning the cell number to be seeded into 4 inoculations performed at 5 day intervals) resulted in constructs with different osteogenic cell progenies. Specifically, constructs with higher seeding densities in the first cell inoculation reached earlier maturation.

Distinct subpopulations, spindle- and round-shape cells, could be morphologically detected only in the periodically seeded niches (*i.e.,* niches #1 and #2), while only round-shape cells were found in constructs grown with the traditional method (*i.e.,* niche #3). Different cellular morphotypes were found to be associated with different expression levels of osteogenic proteins, thus enabling microenvironmental diversification of the niches. In particular, an enhanced expression of OCN, Coll I fibers and nuclear-level Runx2 was found in round cells, while high cytoplasmatic expression of Runx2 was shown by the elongated cells. Among these three niche-groups, niche #2 accounted for the highest surface viability, most regular inner colonization and statistically significant difference between live and dead cells over the third dimension. Finally, niche #2 showed calcium content not statistically different from the traditional method (100.03 ± 29.30 *vs.* 78.51 ± 28.50 pg/cell, respectively; $p =$ n.s.) but, unlike niche #3, it gained a reservoir of non-terminally differentiated cells (*i.e.,* 40.8% of spindle-like cells), potentially able to maintain self-renewal and to pulse further maturation of the construct. Niche #2 can thus be considered an interesting and efficient alternative to the traditional bone-TE substitutes.

Acknowledgements

Author Disclosure Statement

No competing financial interests exist.

References

1. Bianco, P., Robey, P.G., and Simmons, P.J. Mesenchymal stem cells: Revisiting history, concepts, and assays. Cell Stem Cell **2**, 313, 2008.

2. Aubin, J.E. Bone Stem Cells. J Cell Biochem **S30/S31**, 73, 1998.

3. Scadden, D.T. The stem-cell niche as an entity of action. Nature **441,** 1075, 2006.

4. Bianco, P., and Robey, P.G. Stem cells in tissue engineering. Nature **414**, 118, 2001.

5. Barrilleaux, B., Phinney, D.G., Prockop, D.J., and O'connor, K.C. Review: Ex Vivo Engineering of Living Tissues with Adult Stem Cells. Tissue Eng **12**, 3007, 2006.

6. Jaiswal N., Haynesworth S.E., Caplan A.I., and Bruder S.P. Osteogenic differentiation of purified, culture-expanded human mesenchymal stem cells in vitro. J Cell Biochem **64**, 295, 1997.

7. Kasper, F.K., Liao, J., Kretlow, J.D., Sikavitsas, V.I., and Mikos, A.G. Flow perfusion culture of mesenchymal stem cells for bone tissue engineering. StemBook, ed. The Stem Cell Research Community, 2008 http://www.stembook.org.

8. Gregory, C.A., Ylostalo, J., and Prockop, D.J. Adult bone marrow stem/progenitor cells (MSCs) are preconditioned by microenvironmental "niches" in culture: a two-stage hypothesis for regulation of MSC fate. Sci STKE **294**, 37, 2005.

9. Grayson, W.L., Martens, T.P., Eng, G.M., Radisic, M., and Vunjak-Novakovic, G. Biomimetic approach to tissue engineering. Semin Cell Dev Biology **20,** 665, 2009.

10. Ingber, D.E., Mow, V.C., Butler, D., Niklason, L., Huard, J., Mao, J., Yannas, I., Kaplan, D., and Vunjak-Novakovic, G. Tissue Engineering and Developmental Biology: Going Biomimetic. Tissue Eng **12**, 3265, 2006.

11. Chen, X.D., Dusevich, V., Feng, J.Q., Manolagas, S.C., and Jilka, R.L. Extracellular matrix made by bone marrow cells facilitates expansion of marrow-derived mesenchymal progenitor cells and prevents their differentiation into osteoblasts. J Bone Miner Res **22**, 1943, 2007.

12. Mauney, J.R., Kirker-Head, C., Abrahamson, L., Gronowicz, G., Volloch, V., and Kaplan, D.L. Matrix-mediated retention of in vitro osteogenic differentiation potential and in vivo bone-forming capacity by human adult bone marrow-derived mesenchymal stem cells during ex vivo expansion. J Biomed Mater Res A **79**, 464, 2006.

13. Liao, J., Hammerick, K.E., Challen, G.A., Goodell, M.A., Kasper, F.K., and Mikos, A.G. Investigating the role of hematopoietic stem and progenitor cells in regulating the osteogenic differentiation of mesenchymal stem cells in vitro. J Orthop Res **29**, 1544, 2011.

14. Kim, K., Dean, D., Mikos, A.G., and Fisher, J.P. Effect of initial cell seeding density on early osteogenic signal expression of rat bone marrow stromal cells cultured on cross-linked Poly(propylene fumarate) disks. Biomacromol **10**, 1810, 2009.

15. Issa, R.I., Engebretson, B., Rustom, L., McFetridge, P.S., and Sikavitsas, V.I. The effect of cell seeding density on the cellular and mechanical properties of a mechanostimulated tissue-engineered tendon. Tissue Eng Part A **17**, 1479, 2011.

16. Mattii, L., Battolla, B., D'Alessandro, D., Trombi, L., Pacini, S., Cascone, M.G., Lazzeri, L., Bernardini, N., Dolfi, A., Galimberti, S., and Petrini, M. Gelatin/PLLA sponge-like scaffolds allow proliferation and osteogenic differentiation of human mesenchymal stromal cells. Macromol Biosci **8**, 819, 2008.

17. Danti, S., Lisanti, M., Berrettini, S., Petrini M., and Pietrabissa, A. Bone tissue engineering: natural origination or synthetic polymeric scaffolds? Adv Mater Res **15-17**, 65, 2007.

18. Danti, S., Rizzo, C., Polacco, G., Cascone, M.G., Giusti, P., and Lisanti, M. Design of an advanced temporary hip prosthesis for an effective recovery of septic mobilizations: a preliminary study. Int J Artif Organs **30**, 939, 2007.

19. Lazzeri L, Cascone MG, Danti, S., Serino, L.P., Moscato, S., and Bernardini, N. Gelatine/PLLA sponge-like scaffolds: Morphological and biological characterization. J Mater Sci Mater Med **18**, 1399, 2007.

20. Arvidson K, Abdallah BM, Applegate LA, Baldini N, Cenni E, Gomez-Barrena E, Granchi D, Kassem M, Konttinen YT, Mustafa K, Pioletti DP, Sillat T, Finne-Wistrand A. Bone regeneration and stem cells. J Cell Mol Med, **15**, 718-46, 2011.

21. Repetto G, del Peso A, Zurita JL. Neutral red uptake assay for the estimation of cell viability/cytotoxicity. Nat Protoc **3**, 1125, 2008.

22. http://rsbweb.nih.gov/ij/index.html

23. http://www.R-project.org

24. Danti, S., D'Alessandro, D., Pietrabissa, A., Petrini, M., and Berrettini, S. Development of tissue-engineered substitutes of the ear ossicles: PORP-shaped poly(propylene fumarate)-based scaffolds cultured with human mesenchymal stromal cells. J Biomed Mater Res A **92**, 1343, 2010.

25. Singer, V.L., Jones, L.J., Yue, S.T., and Haugland, R.P. Characterization of PicoGreen reagent and development of a fluorescence based solution assay for double-stranded DNA quantitation. Anal Biochem **249**, 228, 1997.

26. Taylor, S.R., Titus-Ernstoff, L., and Stitely, S. Central values and variation of measured nuclear DNA content in imprints of normal tissues determined by image analysis. Cytometry **10**, 382, 1989.

27. Bretaudiere, J.P., and Spillman, T. Alkaline phosphatases, routine method. In: Bergmeyer, H.U., Bergmeyer, J., and Graßl, M., eds. Methods of Enzymatic Analysis. Deerfield Beach, FL: Verlag Chemie, 1984, pp. 75-82.

28. Milch, R.A., Rall, D.P., and Tobie, J.E. Fluorescence of Tetracycline Antibiotics in Bone. J Bone Joint Surg Am **40**, 897, 1958.

29. Martins, A.M., Saraf, A., Sousa, R.A., Alves, C.M., Mikos, A.G., Kasper, F.K., and Reis, R.L. Combination of enzymes and flow perfusion conditions improves osteogenic differentiation of bone marrow stromal cells cultured upon starch/poly(epsilon-caprolactone) fiber meshes. J Biomed Mater Res A **94**, 1061, 2010.

30. Van Den Dolder, J., Spauwen, P., and Jansen, J.A. Evaluation of Various Seeding Techniques for Culturing Osteogenic Cells on Titanium Fiber Mesh. Tissue Eng **9**, 315, 2003.

31. Stein, G.S., and Lian, J.B. Molecular mechanisms mediating proliferation/differentiation interrelationships during progressive development of the osteoblast phenotype. Endocr Rev **14**, 424, 1993.

32. Qui, X., Liu, J., Chang, X., and Xu, X. Comparative study on seeding methods of human bone marrow stromal cells in bone tissue engineering. Chin Med J **117**, 576, 2004.

33. Alvarez-Barreto, J.F., Linehan, S.M., Shambaugh, R.L., and Sikavitsas, V.I. Flow Perfusion Improves Seeding of Tissue Engineering Scaffolds with Different Architectures. Ann Biomed Eng **35**, 429, 2007.

34. Hoemann, C.D., El-Gabalawy, H., and McKee, M.D. In vitro osteogenesis assays: influence of the primary cell source on alkaline phosphatase activity and mineralization. Pathol Biol (Paris) **57**, 318, 2009.

35. Wendt, D., Marsano, A., Jakob M., Heberer M., and Martin I. Oscillating Perfusion of Cell Suspensions Through Three-Dimensional Scaffolds Enhances Cell Seeding Efficiency and Uniformity. Biotechnol Bioeng **84**, 205, 2003.

36. Lian, J.B., and Stein, G.S. Development of the osteoblast phenotype: molecular mechanisms mediating osteoblast growth and differentiation. Iowa Orthop J **15**, 118, 1995.

37. Aubin, J.E. Advances in the osteoblast lineage. Biochem Cell Biol **76**, 899, 1998.

38. Kerr, J.F., Wyllie, A.H., and Currie A.R. Apoptosis: a basic biological phenomenon with wide-ranging implications in tissue kinetics. Br J Cancer **26**, 239, 1972.

Captions
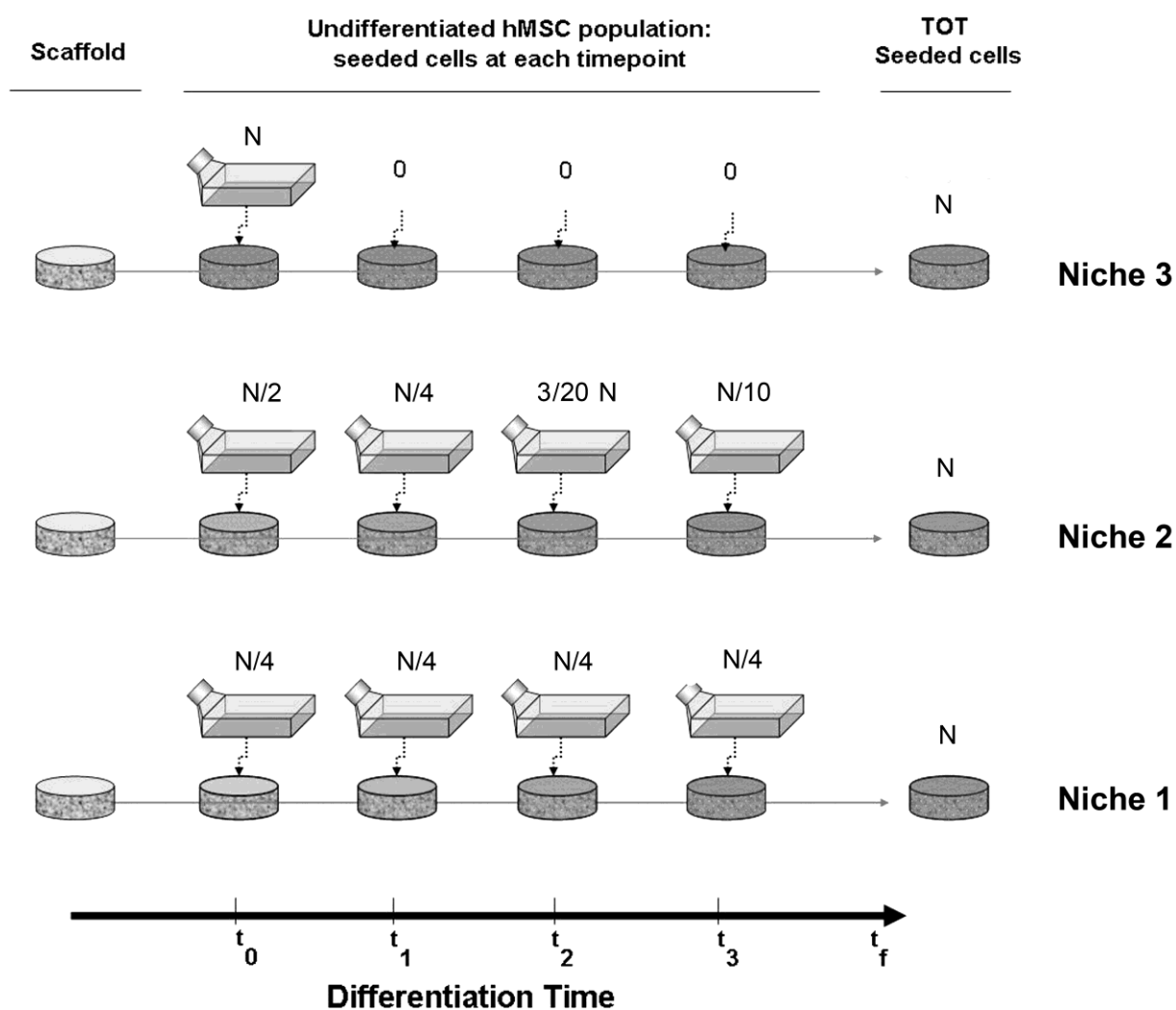
Figure 1

Schematic of dynamic hMSC/scaffold assembly leading to 3 different osteogenic niches at an endpoint (t_f). In each niche type, the total number (N) of undifferentiated hMSCs to be seeded is time-fractioned in 4 seeding shots to be inoculated at time intervals (t_0, t_1, t_2, t_3), with specific cell densities for each group. Niche #1 is periodically seeded with constant-density cell shots, niche #2 with decreasing-density cell shots and niche #3 with the traditional seeding mode (all cells in one shot). In the three cases described in this study, the seeded cells *per* scaffolds and the specific times used are reported in Table 1.

$t_0 + 1$ day $t_3 + 1$ day

Niche 1   A1   A2

Niche 2   B1   B2

Niche 3   C1   C2

3 mm
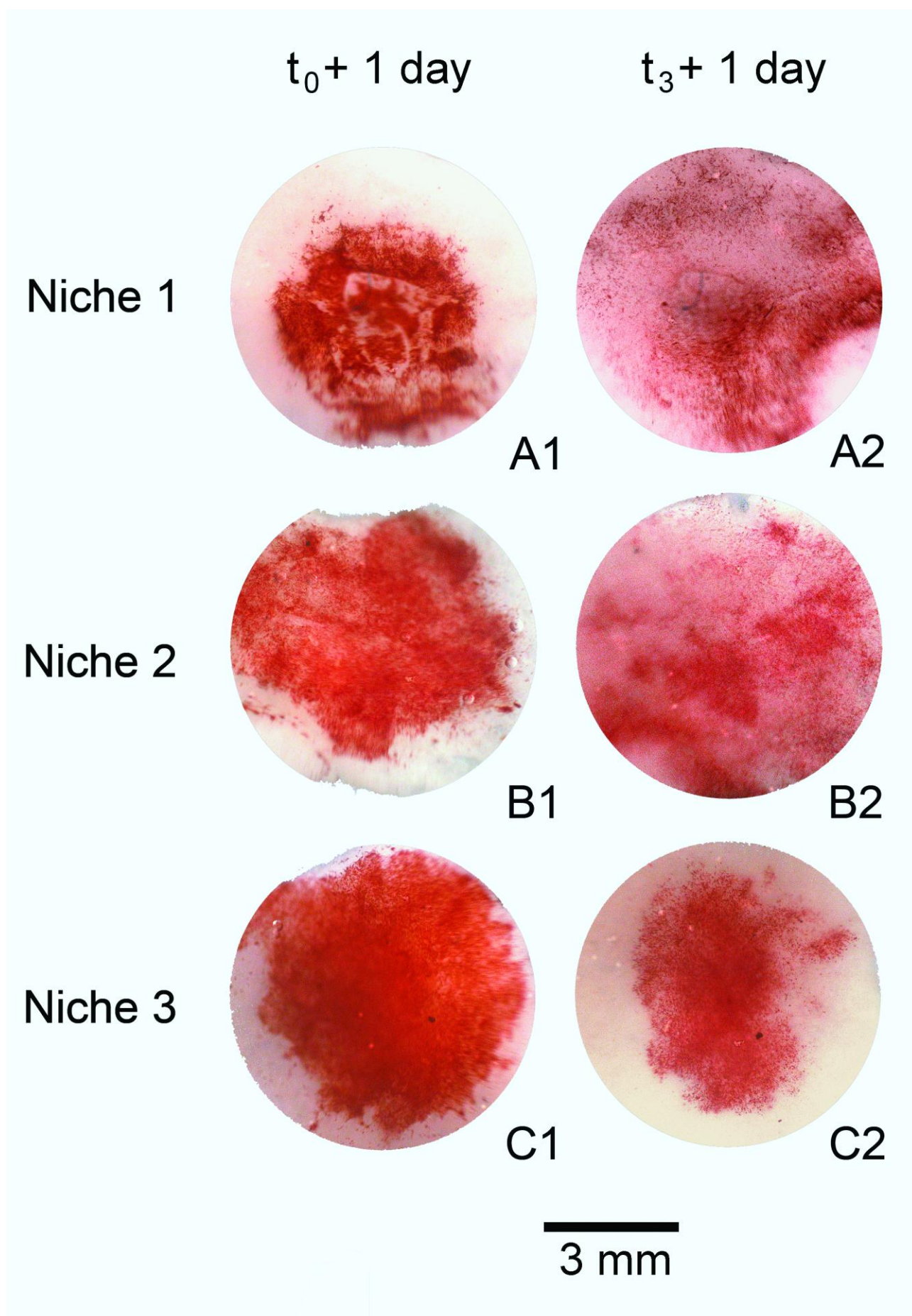
Figure 2

Surface viability of the niches: Stereomicroscopy images of the NR assay showing viable cells (in red) on the top surfaces of the same samples observed at two different time-points. (**A1-C1**) Samples on day 2, (*i.e.,* 1 day after the 1st cell-shot). (**A2-C2**) Samples on day 16 (*i.e.,* 1 day after the last cell-shot).
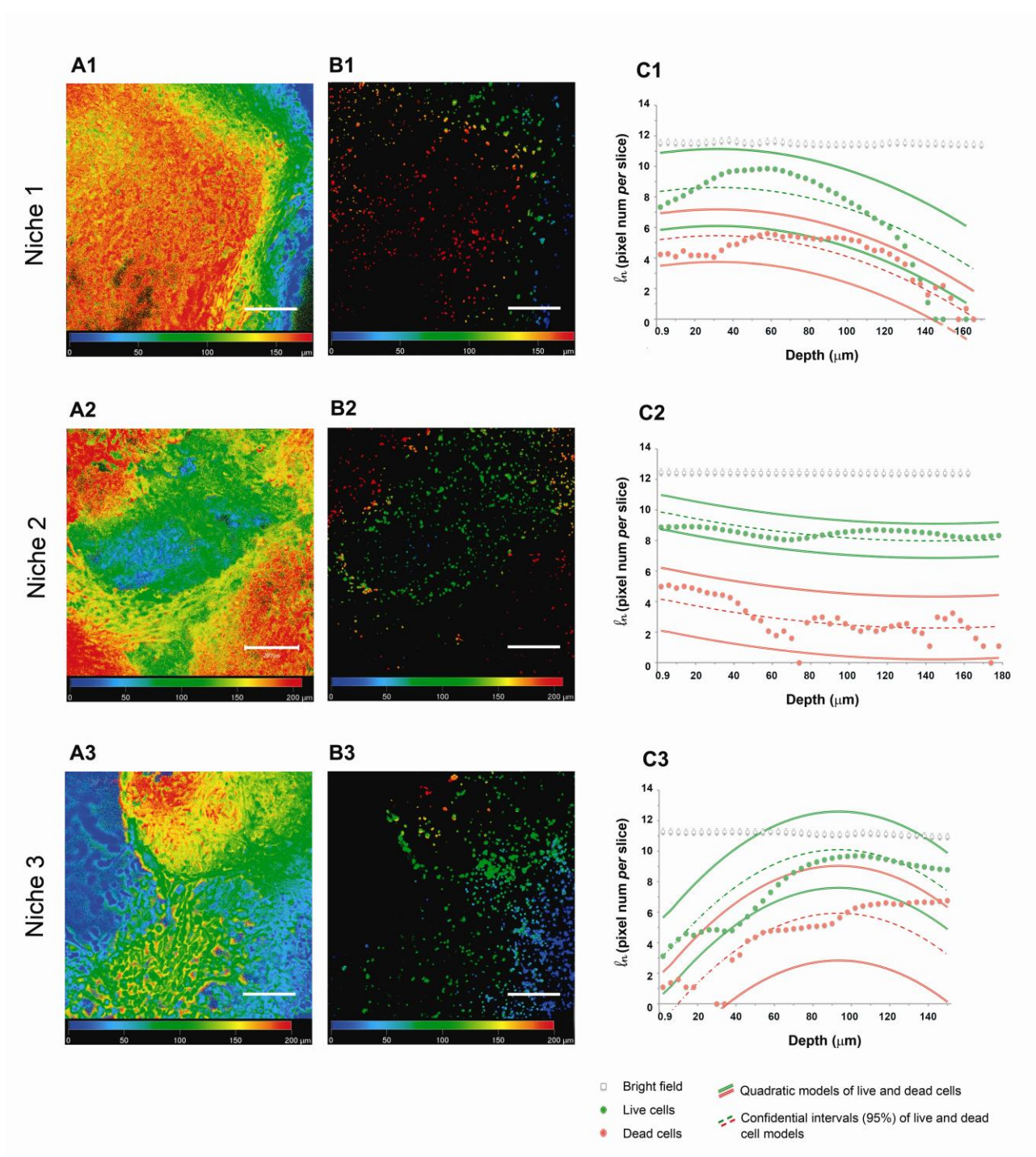
Figure 3

3D viability of the niches: viable and dead cells at t_f. (**A-B**) Results of Live/Dead[®] assay *via* CLSM

rendered using the "depth code" mode up to about 200 μm depth (colored scale bars for z axis).

White scale bar (for xy plane) is 200 μm. (**A1-3**) Live cell colonization. (**B1-3**) Dead cell

localization. (**C**) Results of image analysis performed on the CLSM sections for each depth level

and color channel at maximum intensity, fitted with a polynomial regression and statistically evaluated. (**C1-3**) Graphs show the logarithmic progression of the pixel number for live and dead cells over the sample thickness (z axis) and the related confident intervals.
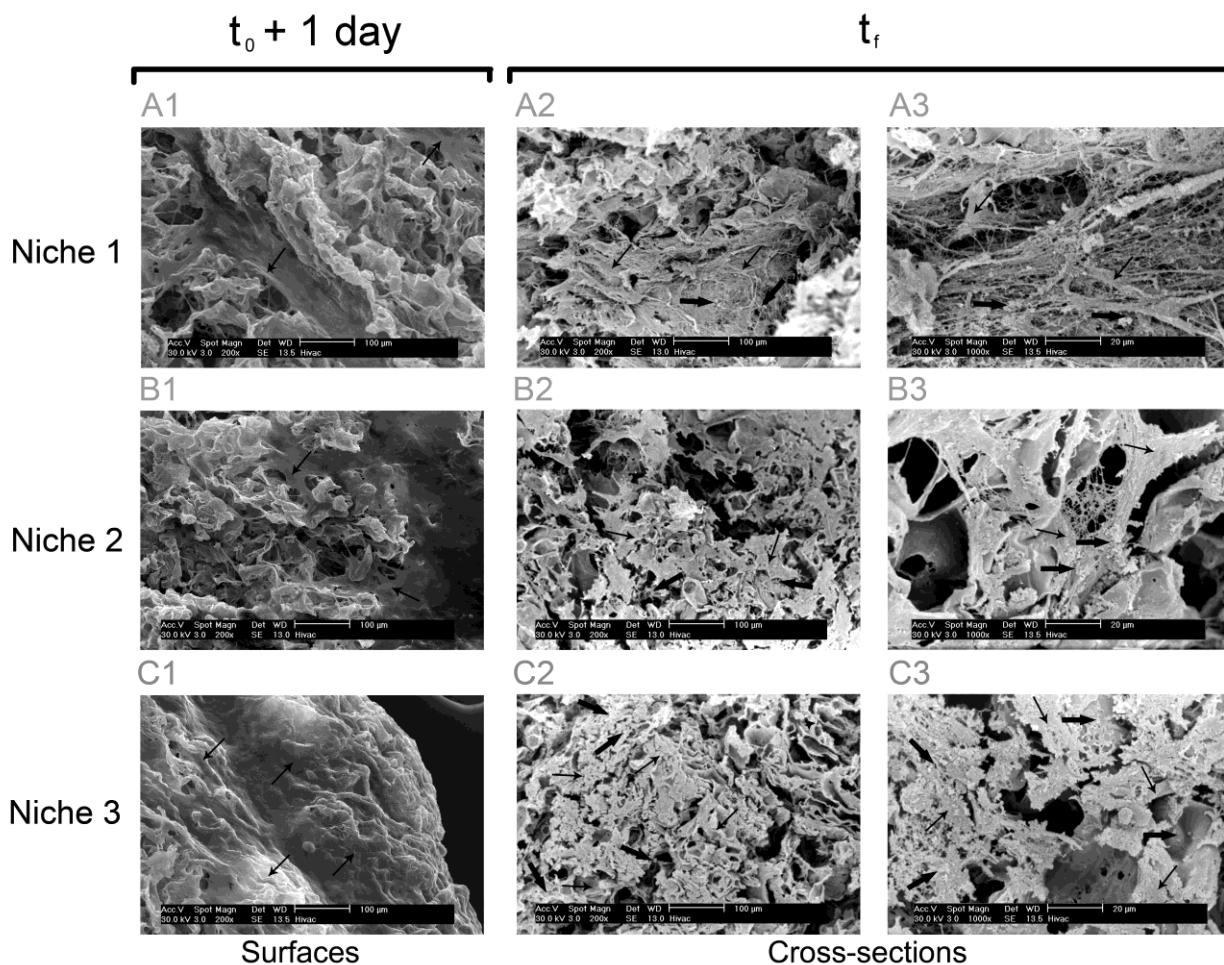
Figure 4

SEM micrographs of the three niches on day 2 [*i.e.,* (t_0 + 1 day)] and on day 21 [*i.e.,* endpoint or (t_f)]. Thin and thick arrows indicate cells and ECM, respectively. (**A1-C1**) Micrographs on day 2, showing the hMSC colonization of the top surfaces; magnification 200×, scale bar 100 μm. (**A2-C2**) Micrographs at the endpoint (t_f), showing cell colonization and ECM production by osteo-differentiated hMSCs in cross-sections (magnification 200×, scale bar 100 μm). (**A3-C3**) Inner section micrographs at the endpoint (t_f), highlighting cell morphology and ECM production; (magnification 1,000×, scale bar 20 μm).

A

Cellularity

B

**ALP activity**

C

Calcium content
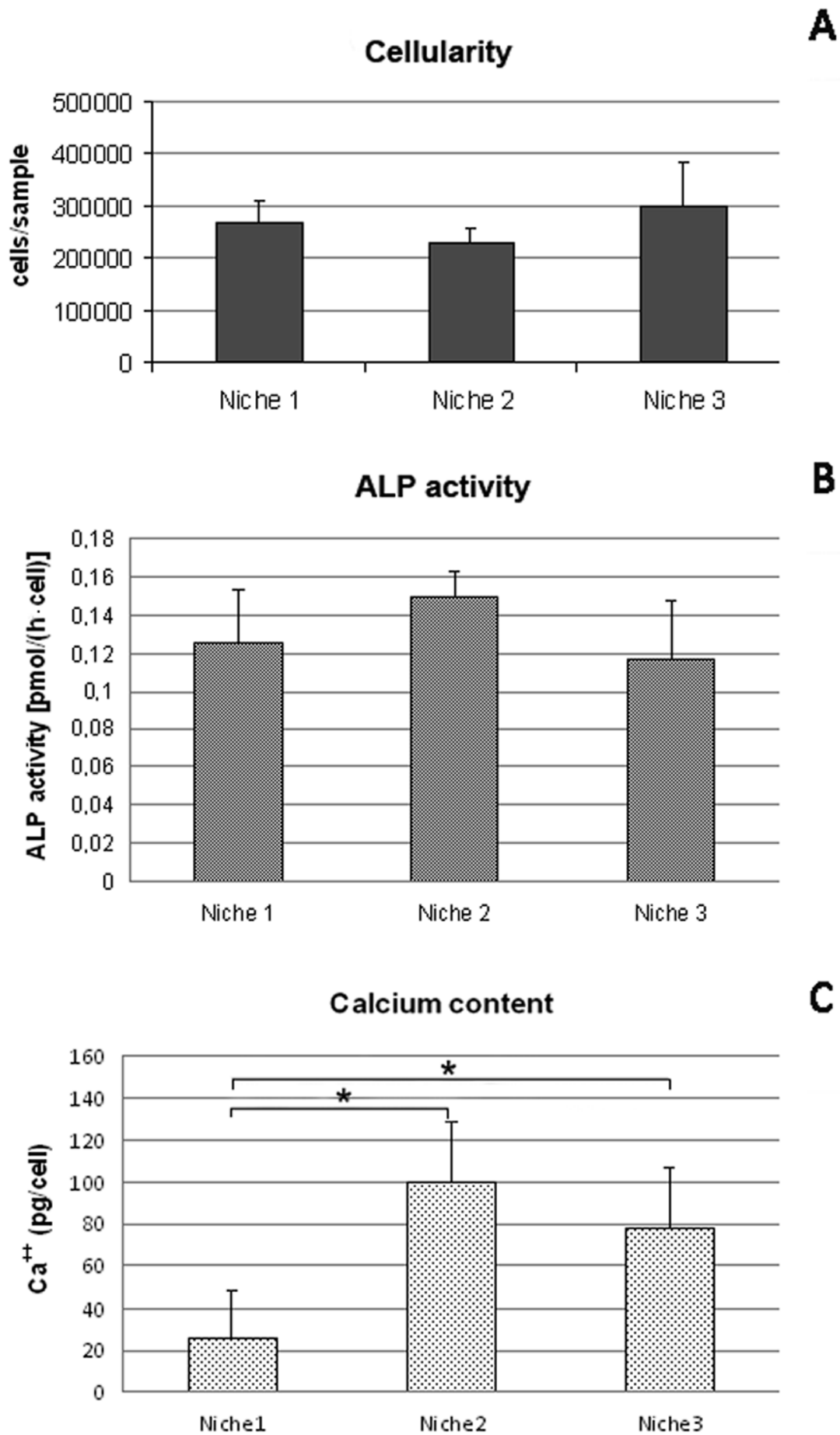
Figure 5

Bar graphs of quantitative analyses performed in quadruplicate ($n = 4$) and in succession on the same construct lysates of the three niches at the endpoint (t_f). (**A**) Cellularity obtained by ds-DNA quantification, assuming 7.18 pg of DNA *per* hMSC. The detected differences are not statistically significant (p = n.s.). (**B**) Intracellular ALP activity shows not statistically significant values (p = n.s.). (**C**) Calcium content after final acid incubation of the constructs. Statistically significant differences are detected between niche #1 and #2, and between niche #1 and #3 ($p<0.01$ in both comparisons). None statistically significant difference is found between niche #2 and #3 (p = n.s.).
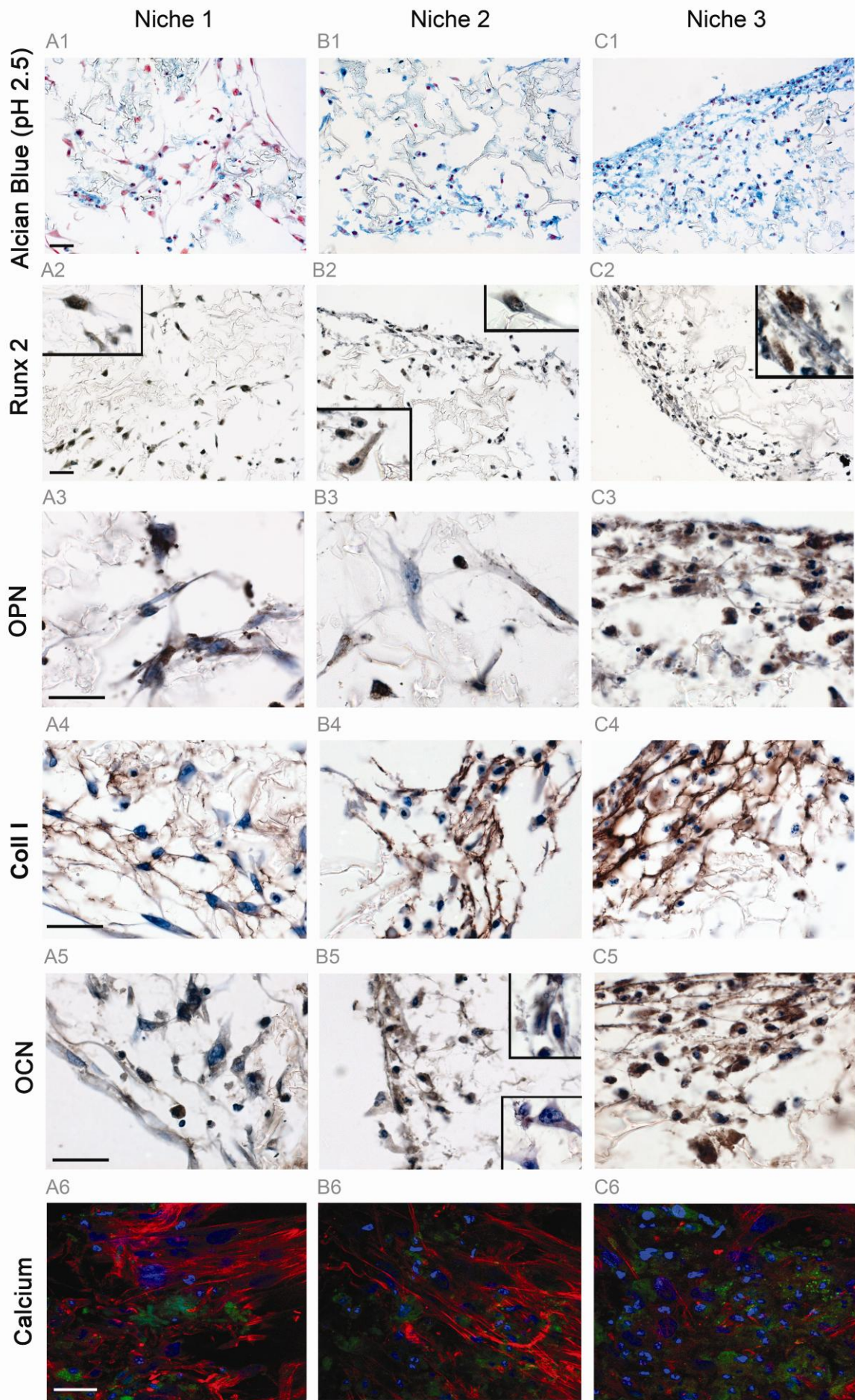
Figure 6

(1-5 A-C) Light microscopy images of inner sections of niches #1, #2, #3 (A, B, C, respectively) at the endpoint (t_f). Magnifications are expressed as the ocular magnification ($10\times$) multiplied by the objective magnifications. These micrographs are representative of about 10–12 sections per staining/antigen type performed at different depths of constructs. **(A1–C1)** Alcian Blue staining at pH 2.5, showing the presence of generic acid GAGs in cyan blue and cell nuclei in red, magnification $400\times$. **(2-5 A-C)** Osteogenic proteins *via* immunohistochemistry. Antigens are revealed in brown. **(A2–C2)** Runx2 expression, magnification $400\times$. Insets show examples of nuclear/cytoplasm localizations, magnification $1,000\times$. **(A3–C3)** OPN expression, magnification $1000\times$. **(A4–C4)** Coll I expression, magnification $1,000\times$. **(A5–C5)** OCN expression, magnification $1000\times$. Insets show different OPN intensity in niche #2, magnification $1,000\times$**(B5)**. **(6 A-C)** CLSM images of inner sections of niches #1, #2, #3 (A, B, C, respectively), magnification $600\times$. These micrographs are representative of about 5-7 sections performed at different depths of constructs. Calcium is stained in green, f-actin in red and nuclei in blue. **(1-6 A-C)** Scale bar 30 μm.
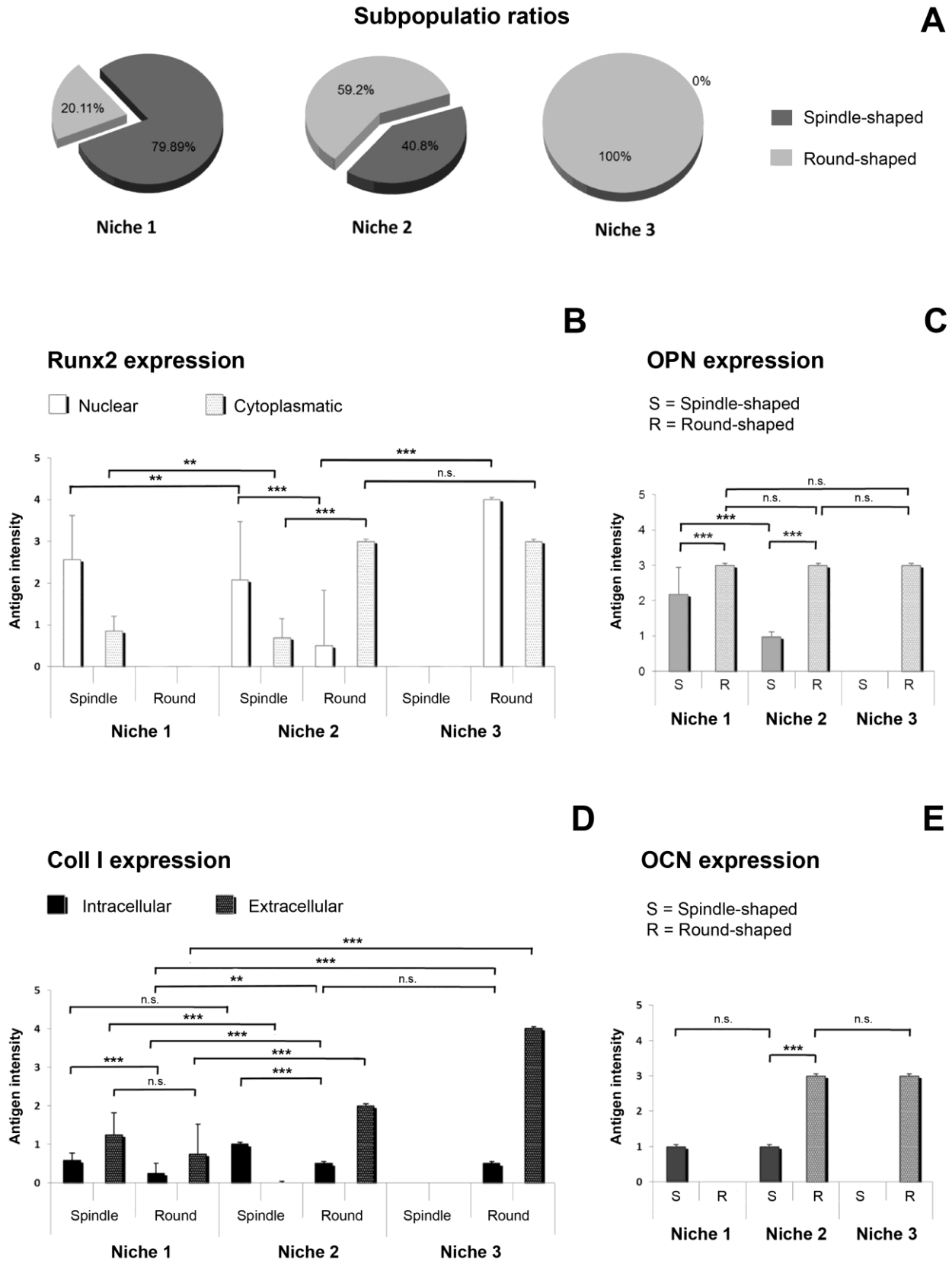
Figure 7

Bar graphs showing semiquantification of cell morphotypes and related proteic markers at the endpoint (t_f). Averages of about 600 cells were counted and analyzed for each niche-type, using light microscopy micrographs at $40\times$ optical magnification (total magnification $400\times$). **(A)** Pie graphs representing the percentage ratio between spindle-like and round morphotypes in the niches. **(B-E)** Intensity of osteogenic antigens in the niches. **(B)** Runx2 intensity and localization in the different cell morphotypes of the niches. **(C)** OPN intensity in the different cell morphotypes of the niches. **(D)** Coll I intensity and localization in the different cell morphotypes of the niches. **(E)** OCN intensity in the different cell morphotypes of the niches.

Antigen positivity was scored by 3 independent observers according to the following criteria: 0 = negative; 1 = weak; 2 = good; 3 = strong; 4 = very strong. Error bars indicate scoring differences due to non-homogeneous expression of the antigen within the specific morphotype/niche. Asterisk indicates statistical significance (*, ** and *** indicate $p = 0.01$, $p = 0.001$ and $p = 0.0001$, respectively), while "n.s." indicates not statistically significance of comparisons.

Table 1

Seeding parameters

Niche #	Number of seeded cells at each seeding time				TOT seeded cells/sample	Seeding efficiency
	t_0 = day 0	t_1 = day 5	t_2 = day 10	t_3 = day 15		
1	125,000	125,000	125,000	125,000	500,000	91.08 %
2	250,000	125,000	75,000	50,000	500,000	93.27 %
3	500,000	0	0	0	500,000	90.49 %

Table 2

Regressive model coefficients for the equation $Y = (a + \gamma_s) + bX + cX^2$.

Niche #	a	b	c	γ_{red}	γ_{green}
1	1.098	0.00178	-0.0003	4.099	7.253
2	1.372	-0.02664	$9.319 \cdot 10^{-5}$	2.806	8.510
3	-5.814	0.15509	-0.0008	4.660	7.539
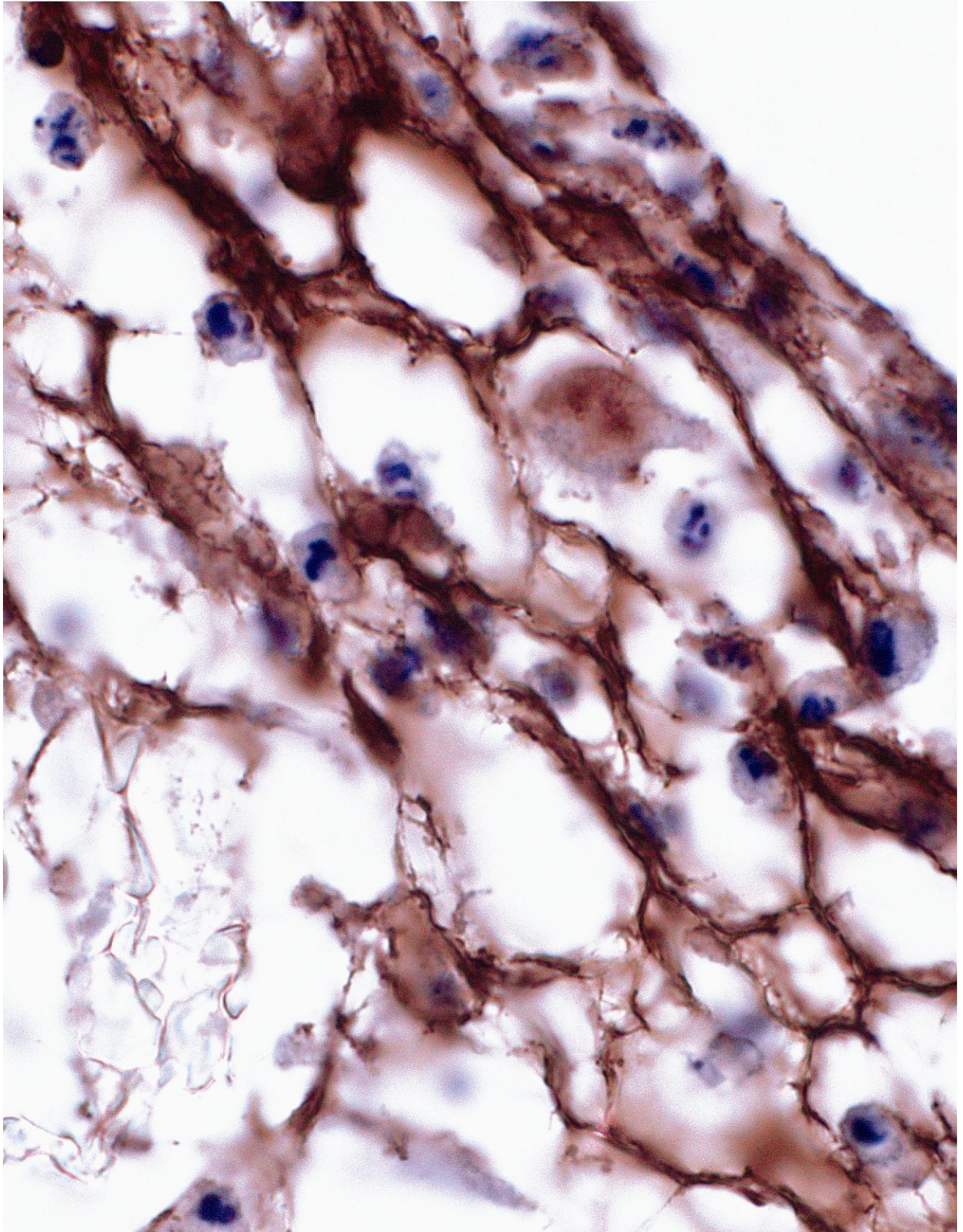
 Potential journal cover (Figure 6 C4)

Coll I expression in niche 3 via immunohistochemistry. Magnification 1,000 x.